Journal of Membrane Science 470 (2014) 40–51

Contents lists available at ScienceDirect

Journal of Membrane Science

journal homepage: www.elsevier.com/locate/memsci

Characterization of ultrafiltration membranes fouled by quantum dots by confocal laser scanning microscopy

N. Wu [a,1], Y. Wyart [a], L. Siozade [b], G. Georges [b], P. Moulin [a,*]

[a] Aix Marseille Université, CNRS, Centrale Marseille, M2P2 UMR 7340, Equipe Procédés Membranaires (EPM), Europôle de l'Arbois, BP80, Pavillon Laennec, Hall C, 13545 Aix en Provence Cedex, France

[b] Aix Marseille Université, CNRS, Centrale Marseille, Institut FRESNEL, UMR 7249, Campus Universitaire de St Jérôme, 13397 Marseille Cedex 20, France

ARTICLE INFO

Article history:
Received 24 January 2014
Received in revised form
25 June 2014
Accepted 1 July 2014
Available online 14 July 2014

Keywords:
Nanoparticle
Membrane filtration
Confocal microscopy
Fouling

ABSTRACT

The extensive applications of engineered nanomaterials (ENMs) can result in their release into waters. Membrane processes have great potential in reducing ENMs release. In that case, the issues of particular concern are membrane fouling caused by ENMs during separation processes. The objective of the present study is to improve the understanding of how ENMs are retained by membranes. An innovative methodology using confocal laser scanning microscopy (CSLM) is developed to locate fluorescent CdTe quantum dots (QDs) in different depths of fouled ultrafiltration membranes. With the help of image analysis software, both qualitative and quantitative information about the distribution of QDs in membranes are obtained. For low molecular weight cut off (MWCO) membranes (1, 5 and 10 kDa), QDs (sizes from 1 to 5 nm) distributed mainly around surfaces or on top of membranes, accompanied with near 100% retention regardless of transmembrane pressure. As membrane MWCO increased (30 and 100 kDa), more QDs could pass through membranes accompanied with decreasing retention efficiencies and the occurrence of QDs was usually in deeper positions of membranes. Distribution results were in agreement with fouling analysis which demonstrated that standard blocking (internal fouling) and/or cake models (external fouling) frequently occurred during filtrations of QDs.

1. Introduction

The rapid development of nanotechnology allows engineered nanomaterials (ENMs) to be widely used in various industrial and commercial products. However, the extensive applications of ENMs will inevitably result in their release into waters, and thereby lead to the exposure of living organisms, as well as humans (e.g. by drinking water consumption and food chain transfer) [1,2]. More and more researchers are concerned about the occurrence, behavior and fate of these emerging contaminants in water environment, as well as their removal/separation technologies.

The use of membrane filtration processes in the study of ENMs is interesting and promising. Membrane filtrations cannot only be used as fractionation techniques prior to further analysis, but also used to remove or separate ENMs from suspensions [2]. Particularly membrane processes are being increasingly used in water treatment processes, such as the extensive applications of ultrafiltration (UF) membranes in drinking water treatment. However, there is still a large knowledge gap on the efficiencies of membrane filtrations in removing ENMs [3,4]. It is urgently needed to investigate the behaviors of ENMs during filtration processes: retention, adsorption onto membrane surfaces, entrapment within membrane pores or passage through membranes, and their impact on membrane fouling or on backwash efficiency.

The separation of ENMs from suspensions through membrane filtration processes are usually challenged by membrane fouling problems [5,6]. Thus, it was decided to study the membrane fouling caused by ENMs, in order to better understand the locations where ENMs are retained (inside membranes or on their surfaces), and to predict the possibility of backwash in removing/reducing membrane fouling. One type of ENMs, the fluorescent semiconductor nanocrystals, also known as quantum dots (QDs), were selected for this study. Because QDs can exhibit size dependent tunable photoluminescence with narrow emission bands, as well as broad absorption spectra [7]. Additionally, QDs are very promising fluorescent markers, due to their good biocompatibility, strong photostability and high quantum yield [8,9].

The fluorescence of QDs can be detected by confocal laser scanning microscopy (CLSM), which is a non-destructive visualization technique without requiring pretreatment of samples. CLSM can provide images at different depths of a 3-dimensional object, and allow the visualization of fouling at membrane surfaces and also inside the porous matrix [10]. To enhance the contrast of

* Corresponding author. Tel.: +33 4 42 90 85 01; fax: +33 4 42 90 85 15.
E-mail address: philippe.moulin@univ-amu.fr (P. Moulin).
[1] Present address: College of Engineering and Technology, Tianjin Agricultural University, 300384 Tianjin, PR China.

http://dx.doi.org/10.1016/j.memsci.2014.07.001
0376-7388/

images, CLSM normally requires that samples are inherently fluorescent or stained with fluorescent reagents. However, the influence of fluorescent dyes on membrane fouling could be significant [11]. The fluorescent properties of QDs allow their application in membrane fouling characterization directly without staining, consequently avoiding the possible influence of fluorescent reagents on the target samples.

Despite that CLSM suffers from low resolution and limited penetration depth, it has been successfully applied in many fields, such as characterization of biofouling in flat sheet membranes [10,12], hollow fiber membranes [13–15] and membrane bioreactor [16]. However, very few studies have been reported on the application of CLSM in membrane fouling characterization during filtration of ENMs, and only qualitative information was obtained [5].

The objective of this study was to apply CLSM to locate fluorescent QDs in different depths of fouled membranes, with the help of image analysis software. Five types of CdTe QDs with different sizes and five UF membranes with different molecular weight cut off (MWCO) were tested in a dead-end filtration system under the conditions of two transmembrane pressures (TMP). The impact of membrane MWCO and TMP on retention and recovery efficiencies of QDs was also assessed. The results obtained improve the understanding of how ENMs are retained by membranes and give more insights into the impact of membrane fouling on separation of ENMs.

2. Materials and methods

2.1. Preparation of QDs suspensions

Hydrophilic CdTe QDs (powders) coated with a proprietary mixture of low-molecular weight thiocarboxylic acid (PlasmaChem GmbH, Germany) were used to prepare suspensions to be filtered. Five types of CdTe QDs with different maximum emission wavelengths at $\lambda = 510 \pm 5$ nm (CdTe-510), $\lambda = 530 \pm 5$ nm (CdTe-530), $\lambda = 580 \pm 5$ nm (CdTe-580), $\lambda = 650 \pm 5$ nm (CdTe-650) and $\lambda = 700 \pm 5$ nm (CdTe-700) were investigated in this study, which correspond to different colors and sizes.

The suspensions were prepared with Milli-Q ultrapure water (pH about 7, conductivity of 0.6 $\mu S\ cm^{-1}$). 50 mL CdTe suspensions were prepared just before the filtration experiments, with a concentration of 100 mg L^{-1}. Among them, 40 mL CdTe were used as feed suspensions to be filtered, and the remaining 10 mL suspensions were used for concentration analysis.

2.2. Characterization of QDs

To obtain information about surface charges of QDs particles in suspensions, zeta potentials were measured using a Zetasizer Nano ZS (Malvern Instruments Ltd., UK). Measurements were performed at 25 °C.

The concentrations of CdTe QDs suspensions before and after filtrations were determined from their fluorescence analyzed by JENWAY 6285 fluorimeter. Relative Fluorescence Units (RFU) were recorded as a function of CdTe concentrations, and these linear relationships were used to determine the QDs concentrations. The excitation wavelength used for RFU analysis was 350 nm, because QDs can be excited with any laser having a wavelength shorter than their maximum emission wavelengths. The emission wavelengths were chosen as a function of nominal maximum emission wavelengths of different CdTe QDs, by changing interference filters in the range from 510 to 700 nm. Since the range of linear relationship between RFU and concentrations was limited, samples with high concentrations which are out of the range of linear relationship, such as retentate and feed, need to be properly diluted before fluorescence analysis.

2.3. Membranes and experimental setup

Five types of flat-sheet disk UF membranes with different MWCO (Ultracel®, Millipore) were evaluated in this study, as shown in Table 1.

Prior to filtration experiments, the membranes were soaked in ultrapure water (Milli-Q) at least 2 h. Then about 50 mL sodium hydroxide (NaOH, pH ≈ 10) solution passed through the membranes, under different pressures according to membrane MWCO. This stage was carried out to remove glycerin on membrane surfaces, which might last about 30 min to more than 1 h. Finally, the membranes were rinsed by ultrapure water (Milli-Q) until the pH of rinsing water being neutral, which was driven by the same pressure as alkaline cleaning procedure. This procedure is in agreement with Millipore requirements.

The filtrations of five QDs were carried out by 1, 5, 10 and 30 kDa membranes at constant TMP of 2 bar, and by 10, 30 and 100 kDa membranes at constant TMP of 0.6 bar. Ultrafiltration experiments were carried out using a lab scale filtration system (Fig. 1), which consists of an air-pressurized feed tank connected to an Amicon 8050 stirred filtration cell (Millipore Corporation, Bedford, MA). The volume and effective filtration area of filtration cell are 50 mL and 13.4 cm^2 respectively. To prevent concentration polarization at the membrane surface, dead-end filtration cell was stirred at 200 rpm using a speed adjustable magnetic stirrer (FB15001, Fisher Scientific). This stirring rate was arbitrary selected as a compromise between the shear stress at the membrane surface and the turbulence in the filtration cell [4]. Filtration was carried out at constant TMP (0.6 and 2 bar). All runs were carried out in a clean white room with air conditioning, where room temperature can be maintained at 20 ± 2 °C. The filtration processes lasted from 3 min (e.g. 100 kDa) to more than

Table 1
Characteristics of membranes (Millipore).

MWCO[a] (kDa)	Code[a]	Estimated pore size[b] (nm)	Permeability ($L\ h^{-1}\ m^{-2}\ bar^{-1}$)[c]	Surface charge at pH 8 (mV)[d]	Other information[a]
1	PLAC	1.58	3.3 ± 0.3	−11.6	– **Membrane material:** regenerated cellulose
5	PLCC	3.72	12.6 ± 1.3	−14.3	– **Support material:** polypropylene nonwoven
10	PLGC	5.37	69 ± 3	−7.5	– **Thickness:** 230 μm
30	PLTK	9.61	335 ± 10	−16.4	
100	PLHK	18.20	607 ± 53	−17.3	

[a] Information supplied by Millipore.
[b] Pore sizes were determined from reference [17].
[c] Membrane permeability was determined using the dead-end filtration apparatus (Amicon 8050, Millipore). Permeate flux was measured as a function of feed pressure from 0.5 to 4 bar. The reported permeability value is the average of results from six separate membrane samples ($T = 20$ °C).
[d] Surface charges were taken from reference [18].

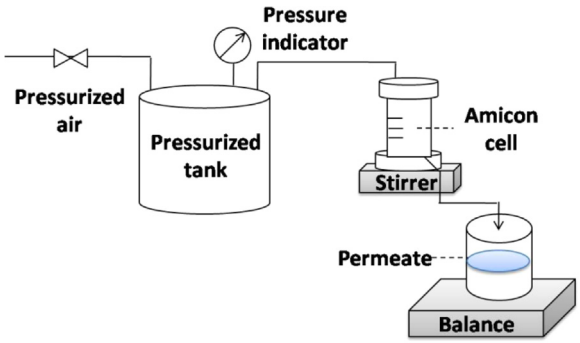

Fig. 1. Schematic diagram of dead-end filtration device for QDs.

4 h (e.g. 1 kDa). The permeate was collected in a beaker placed on an electronic balance ($\Delta m = \pm 0.01$ g) and the filtrate mass data was taken periodically. The permeate collection beaker was wrapped with aluminum foil paper to minimize fluorescence fading of QDs during the filtration runs. The filtration was stopped when the permeate volume reached about 30 mL. The volume concentration factor (the ratio of the initial feed volume to the retentate volume) was about 4.

At the end of filtration, all the retentates and permeates were collected for fluorescence analysis. The volumes of retentates and permeates were recorded for mass balance analyses, which were checked as Eq. (1):

$$(\%\text{recovery}) = (C_p V_p + C_r V_r)/(C_f V_f) \times 100\% \quad (1)$$

where V_f, V_p and V_r are the volumes of feed, permeate and retentate samples, respectively and C_f, C_p and C_r are the concentrations of feed, permeate and retentate samples, respectively.

The retention efficiency was calculated through Eq. (2):

$$(\%\ \text{retention}) = (1 - C_p/C_f) \times 100\% \quad (2)$$

where C_f the feed concentration and C_p the permeate concentration.

2.4. CLSM analysis

Fouled membranes were imaged by CLSM (TCS SP5, Leica Microsystems CMS GmbH, Germany). The membrane samples were first analyzed in reflection mode, in order to determine the position of *z*-axis corresponding to the membrane surface. Then, the fouled membranes were analyzed using the fluorescence mode. Excitation was performed using a 488 nm argon laser (blue, 100% power). Table 2 lists the detection ranges used during CLSM analysis for five types of CdTe QDs. False colors are used to represent the membrane microstructure measured in reflection mode (red color) and QDs fluorescence emission (green color) in the same image.

Membranes were imaged using the *xyz* mode of CLSM, which permits one to scan the *xy* plane along *z*-axis. Images were captured every 5 μm from the outside to the membrane surface, and then to the inside of membrane along 50–100 μm thickness, resulting in a series of 20–30 images for each measurement. In all cases, specimens were magnified using a plan apochromatic 10× objective (NA=0.3), and zoom magnification was set at 1. Images were scanned at 400 Hz, with a resolution of 512 × 512 pixels and an area of 1.10 × 1.10 mm^2. The detection conditions were kept constant for samples obtained at the same filtration conditions.

In order to study the photostability of QDs when exposed to laser during the process of CLSM analysis, assessment was performed by using the *xyt* mode of CLSM. QDs suspensions were illuminated with a 488 nm excitation laser line for about 15 min (100% power, zoom magnification=1). Images were taken at 30 s intervals, with a resolution of 512 × 512 pixels. Region of interest (ROI) of 1.10 × 1.10 mm^2 was selected to show the fluorescence intensity in relation to time. The stability profile analysis was processed using the CLSM software (Leica LAS AF).

Table 2
Physicochemical characteristics of CdTe solutions (100 mg L^{-1}).

QDs	Emission bands (nm)[a]	Size (d nm)[b]	Zeta potential (mV)[c]	Conductivity (mS cm^{-1})[c]
CdTe-510—1.5 nm	500–535	1.53	−29 ± 2	0.034 ± 0.004
CdTe-530—2.2 nm	510–555	2.20	−36 ± 5	0.031 ± 0.002
CdTe-580—3.2 nm	550–610	3.24	−25 ± 5	0.044 ± 0.001
CdTe-650—3.8 nm	625–690	3.75	−27 ± 3	0.040 ± 0.005
CdTe-700—4.5 nm	655–725	4.50	−24 ± 3	0.042 ± 0.014

[a] Detection ranges of emission wavelengths used for CLSM analysis.
[b] Diameters from manufacturers (http://www.plasmachem.com/download/Quantum_dots_sizes_PlasmaChem_GmbH.pdf).
[c] The zeta potential and conductivity values were measured by Zetasizer Nano ZS, solution pH=7.

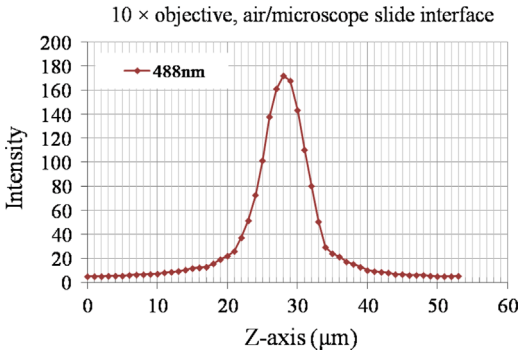

Fig. 2. Profile of air/microscope slide interface, excitation wavelength=488 nm, with a 10× objective.

The resolution values of CLSM can be divided into lateral (*x*–*y*) and axial (*z*) resolution. The lateral resolution depends on the Numerical Aperture (NA) of the objective and the wavelength of excitation source (λ). According to Abbe formula [19], when using a 10× objective (NA=0.3) and blue light with a wavelength of 488 nm, the lateral resolution was about 0.8 μm. In terms of axial (*z*-axis) resolution, it was measured from the air/microscope slide interface profile according to *z*-axis (Fig. 2). Specifically, the axial resolution corresponds to the full width (horizontal axis) at half maximum values of intensity (vertical axis), which was about 7–8 μm.

2.5. Image analysis

The images obtained by CLSM are composed of 512 × 512 pixels with grayscale values ranging from 0 (black) to 255 (white). To calculate the distribution of QDs in different depths of membrane, 'mean intensity' and 'point intensity' methods were used. More details are given in Section 3.5. For 'mean intensity' method, the mean intensity values corresponding to membranes and QDs respectively in an area of 1.10 × 1.10 mm^2 (for each *xy* image) were given by CLSM software (Leica LAS AF). For 'point intensity' method, Image J 1.43 (National Institutes of Health, USA) was used as follows:

File-Import-Image sequence-OK; Image-Stacks-**Reslice**-OK (to obtain *x*–*z* cross sections as a function of *y*).
Color-Split channels (three images with the title of red, green and blue)- choose the color representing the QDs (e.g. green).

Straight (/)-Analyze-Plot Profile (to have a figure of Gray Value as a function of distance)-List-edit- copy the data

Moreover, to generate three-dimensional reconstructed images, the Section mode of Imaris (v7.2.3, Bitplane AG, Zurich, Switzerland) was used.

3. Results and discussion

3.1. Characterization of QDs

The main characteristics of CdTe QDs are summarized in Table 2. The reported sizes of CdTe QDs are in the range of 1–5 nm, growing with the increase of emission wavelengths.

The zeta potential measurements provide the information of surface charges of the particles in suspensions, and also indicate the potential stability of colloidal system. The five types of QDs were strongly negatively charged when dispersed in ultrapure water (pH about 7) that was used in filtration experiments (Table 2). Under these conditions, the QDs suspensions were stable due to the high repulsion forces. Our results are in agreement with researchers [9,20] who demonstrated that QDs terminated with –COOH group had negative charges at pH about 7. As pointed out by Quevedo and Tufenkji [21], the negative surface charge could be attributed to the presence of carboxyl groups in the coatings of QDs. Considering that the surface charges of membranes are also negative under similar pH conditions, there would be less adsorption between QDs and membranes. Further understanding of the surface charges of QDs and membranes will be critical to predict their interactions during filtration processes.

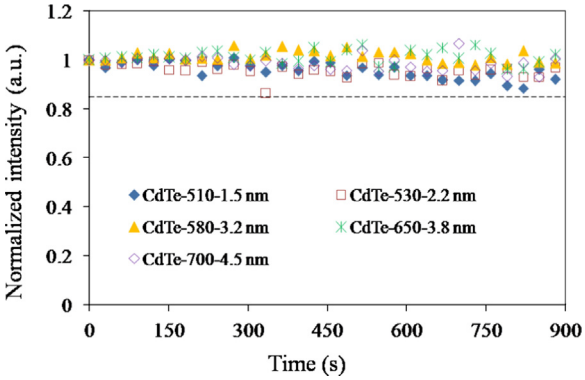

Fig. 3. Photostability profile of CdTe solutions (100 mg L^{-1}) analyzed by CLSM. Profile represents mean intensity as a function of time from 0 to 15 min, excitation wavelength = 488 nm.

To ensure that QDs were photostable during the period of CLSM analysis, their photostabilities were assessed by exposing QDs for 15 min at the maximum power laser line of 488 nm. The exposure time was set for a continuous 15 min, which corresponds to the total detection time during CLSM analysis (4–6 zones scanned for each fouled membrane, about 2 min for each scan). As depicted in Fig. 3, the reductions of fluorescence intensity of all five types of CdTe QDs were less than 15% during 15 min. These results confirmed that QDs are highly photostable, which is in good agreement with Montón et al. [8].

3.2. Retention and recovery efficiencies

Fig. 4 summarizes the retention and recovery results for filtrations of five QDs by different MWCO membranes under two TMP.

3.2.1. Effect of membrane MWCO

At 2 bar (Fig. 4a), whatever the CdTe QDs sizes, they were almost completely retained by 1, 5 and 10 kDa membranes (retention efficiencies close to 100%). But for 30 kDa membranes, a noticeable drop in retention occurred, and the decreasing degree became smaller as QDs sizes increased. For example, from 10 to 30 kDa at 2 bar, a distinct drop in retention from about 100% to

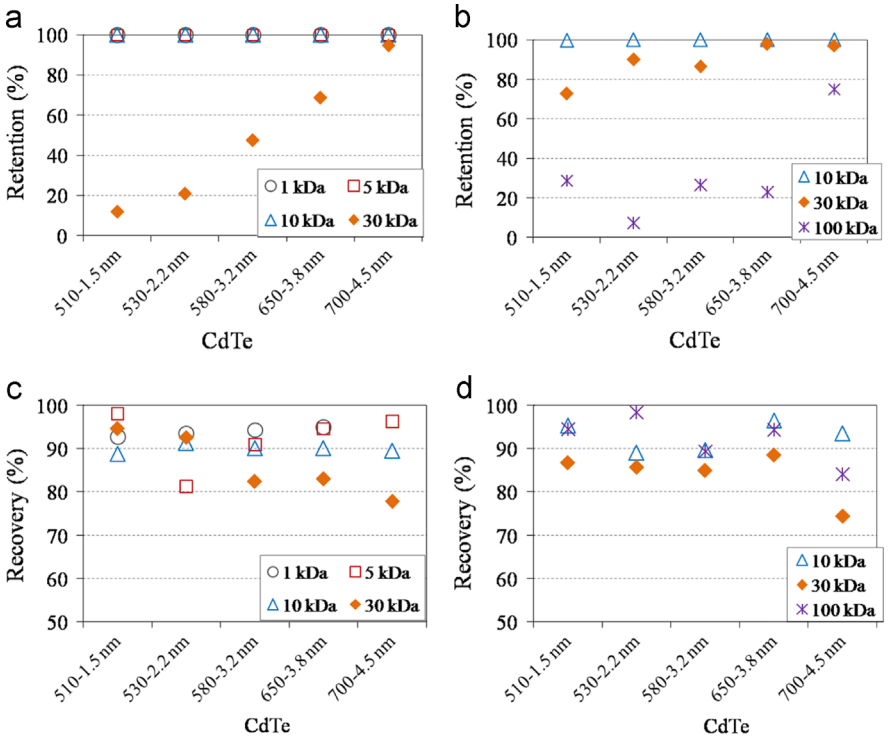

Fig. 4. Retention and recovery efficiencies by different membranes as a function of QDs. (a) Retention-2 bar, (b) Retention-0.6 bar, (c) Recovery-2 bar and (d) Recovery-0.6 bar.

12% was observed for CdTe-510, while only a slight decrease was found for CdTe-700, from 100% to about 95%.

At 0.6 bar, the extent of retention efficiencies generally decreased when membrane pore sizes increase from 10 to 100 kDa (Fig. 4b). Specifically speaking, from 10 to 30 kDa, the noticeable drop in retention was only observed for CdTe-510, 530 and 580; for other two QDs, the decrease in retention was within 3%. At 100 kDa, retention efficiencies of all QDs decreased sharply. However, still about 75% of CdTe-700 was retained by 100 kDa membrane, which displayed significantly higher retention than other QDs (retention efficiencies lower than 30%).

Normally, there was a significant loss from 100% retention efficiency, as membrane MWCO increases from 10 to 30 kDa. When membrane MWCO increases to 100 kDa, small nanoparticles (primary sizes from 1.5 to 3.8 nm) were hardly retained, with retention efficiencies less than 30%. According to these results, it is questionable if UF membranes (e.g. 100–150 kDa) widely used in drinking water treatment can remove nanoparticles efficiently. It cannot be ignored the potential risks associated with low removal efficiencies of ENMs by UF membranes (e.g. 100 kDa). More research should be focused on this part.

Recovery was determined to evaluate if QDs were retained on the basis of size exclusion alone or if they were adsorbed onto membrane surfaces and/or trapped in membrane pores. High recovery is expected when QDs were larger than membrane pores resulting in size exclusion or when QDs were not readily trapped in membrane pores. Low recovery is expected when a considerable fraction of QDs were retained inside the membranes. Recovery efficiencies were over 80%, except for 30 kDa filtrations of CdTe-700 (78% at 2 bar and 75% at 0.6 bar, see Fig. 4c and d). Interestingly for other four QDs, their lowest recovery efficiencies (from 82% to 89%) also occurred at 30 kDa membranes in most cases. Only for CdTe-510 and 530 at 2 bar (Fig. 4c), the lowest recovery efficiencies were found at 10 kDa (89%) and 5 kDa (81%) membranes, respectively.

On the whole, QDs were almost completely retained by low MWCO membranes (1, 5 and 10 kDa) regardless of TMP, and their corresponding recovery efficiencies were generally over 90%. This indicated that QDs were mainly stopped on the low MWCO membrane skins which can be easily recovered, and the retention mechanism could be mainly attributed to size exclusion. Interestingly, the estimated pore size of 10 kDa membranes (5.37 nm, see Table 1) was 3.5 times larger than the reported sizes of CdTe-510 (1.53 nm, see Table 2). There was a possibility that (1) CdTe-510 were entrapped inside porous media of membranes; (2) small aggregates of CdTe-510 formed, which were retained by 10 kDa membranes on the basis of size exclusion. Meanwhile, the entrapment of CdTe-510 within membrane pores also likely occurred contributing to their retention by low MWCO membranes. This hypothesis was in accordance with the low recovery results of CdTe-510 by 10 kDa membranes at 2 bar (89% recovery, see Fig. 4c). But at 0.6 bar, a little more CdTe-510 (about 95%) was recovered during 10 kDa filtration. The possible explanation could be that under low TMP, CdTe-510 was less trapped within 10 kDa membrane pores but more retained outside membranes, compared to the situations under high TMP. More discussion about the impact of TMP on retention and recovery results will be presented in the next section.

As expected, fewer QDs were retained by high MWCO membranes with large estimated pore sizes (9.61 nm for 30 kDa and 18.20 nm for 100 kDa, see Table 1). The larger membrane MWCO/pore sizes, the lower retention efficiencies were observed. Meanwhile, the recovery results revealed that in most cases, the entrapment of QDs within high MWCO membranes (e.g. 30 kDa) occurred more easily than low MWCO membranes. It seems that larger QDs were more entrapped in the porous matrix of 30 kDa membranes according to their lower recoveries (Fig. 4c). But when membrane pores were large enough (100 kDa), QDs could pass through membranes with less entrapment, displaying a high recovery. In this case, the retention efficiencies were usually small, except for larger QDs e.g. CdTe-700 whose retention efficiency strongly increased (Fig. 4b) and recovery was low (Fig. 4d).

3.2.2. Effect of TMP

In order to investigate the impact of TMP on retention and recovery results, two different TMP (2 bar and 0.6 bar) were tested for 10 and 30 kDa membranes, which represent low and high MWCO membranes, respectively. For 10 kDa membranes, retention efficiencies were constant (approximately 100%), which were independent of TMP (Fig. 4a and b). On the contrary, retention of QDs by 30 kDa membranes was largely influenced by the TMP applied. It can be seen that retention efficiencies at 0.6 bar were higher than those at 2 bar during 30 kDa filtration. Meanwhile, the difference between these two retention efficiencies generally diminished as QDs sizes increased. For example, by comparing retention efficiencies in 30 kDa filtrations under two TMP, 61% difference was found for CdTe-510, but almost the same values (only 3% difference) were observed for CdTe-700.

Compared to retention, there was no clear trend about the influence of TMP on recoveries for 10 and 30 kDa membranes, due to the variable values among different QDs (Fig. 4c and d). Generally, recovery efficiencies obtained at 2 bar and 0.6 bar were comparable, and the difference was within 5%. In some cases, up to 8% of variation in recoveries could be observed (e.g. 30 kDa filtration of CdTe-510).

Based on the above results, it appears that TMP had an impact on QDs retention by high MWCO membranes (for 30 kDa in this case), but no effect on retention by low MWCO membranes (for 10 kDa). While for recovery efficiencies, the influence of TMP was not so apparent in most cases.

3.3. Filtration data analysis

The variations of normalized flux (J/J_0) as a function of cumulative permeate volume at TMP of 2 and 0.6 bar were recorded and then analyzed using the classical Hermia laws [22], by plotting the experimental data to the linear forms of four fouling models (cake filtration, intermediate blocking, standard blocking and complete blocking) [6]. For each filtration run, the correlation coefficients (R^2) values of four blocking models are calculated and compared, in order to identify the most appropriate blocking model. According to El Rayess et al. [23], R^2 values should be greater than 0.99 to confirm the model fitting. However, not all R^2 values could meet this requirement in the present study (data not given). This can be explained from two aspects: (1) the classical Hermia law is ideal to be applied in unstirred filtrations, but the filtrations of QDs were performed under 200 rpm stirring conditions; (2) there are some variations in flux decline data due to very small permeate flux (e.g. 1 kDa filtrations). Nevertheless, it was tried to find fitted models with relatively high R^2 values (close to 0.9). These models might present the most possible fouling mechanism for filtration runs.

Table 3 presents the most possible fouling models during 1, 5, 10 and 30 kDa filtration processes (the fouling of 30 kDa—2 bar and 100 kDa–0.6 bar filtrations was not determined due to the lack of data). For each filtration run, fouling models are given when R^2 values are higher than 0.85. Since the models are usually not fitted to the whole stage of filtrations, the fouling models are presented with their corresponding filtration stages (marked with cumulative permeate volumes).

Table 3
Summary of main fouling models corresponding to filtration processes.

	1 kDa–2 bar	5 kDa–2 bar	10 kDa–2 bar	10 kDa–0.6 bar	30 kDa–0.6 bar
CdTe-510—1.5 nm	4–13 mL Standard + Cake**	13–30 mL Standard + Cake**	13–30 mL Standard + Cake**	8–30 mL Intermediate + Complete**	–
CdTe-530—2.2 nm	4–12 mL Standard*	8–30 mL Standard + Cake**	13–30 mL Standard + Cake**	12–30 mL Standard + Cake**	11–30 mL Intermediate + Complete**
CdTe-580—3.2 nm	3–6 mL Standard + Cake**	19–30 mL Standard + Cake**	-	17–30 mL Standard + Cake**	–
CdTe-650—3.8 nm	5–13 mL Standard + Cake**	14–30 mL Standard + Cake**	–	–	–
CdTe-700—4.5 nm	-	13–30 mL Standard + Cake**	–	–	14–30 mL Standard + Cake**

–Cannot be determined.
** R^2 values (≥ 0.9).
* R^2 values (≥ 0.85–0.9).

For all filtration runs in the present study, R^2 values given by standard blocking and cake models were always similar, thus it was possible that two fouling models co-existed. The same case was with intermediate and complete blocking models, which always occurred simultaneously. This result is in agreement with the fact that the classical Hermia models combining two or more blocking mechanisms have been shown to be useful for membranes fouled by more than one mechanism, either sequentially or simultaneously [24]. For 1 kDa membranes, the filtration processes of all QDs can be partially described by standard blocking and/or cake models. Similarly for 5 kDa membranes, the filtrations of all QDs were always described by standard blocking and/or cake models. With regard to 10 and 30 kDa filtrations, they were normally described by standard blocking and/or cake models. Only for CdTe-510 (10 kDa–0.6 bar) and CdTe-530 (30 kDa–0.6 bar), their filtrations were better fitted to intermediate and/or complete blocking models.

Overall, the above results demonstrated that both internal and external fouling might occur during filtration of QDs. The observation of internal fouling was in agreement with recovery results, which revealed that entrapment of QDs within membrane pores possibly occurred contributing to their retention by membranes. Additionally, the internal fouling was also reported to be the prevailing mechanism during microfiltration and ultrafiltration [11,13]. The dominance of cake models revealed that QDs fouling on top of membranes also occurred. These observations will be confirmed by CLSM analysis. However, further studies are needed to get more precise information on fouling mechanisms during filtration of QDs.

3.4. CLSM images of fouled membranes

To identify and locate QDs in membranes, the orthogonal views of 3D structures of fouled membranes are shown in Fig. 5. The reconstructed CLSM images of perpendicular planes (*xy*, *xz*, *yz*) provide the front, top and side views at any given point in the image stacks. Here, examples for images of 1 kDa (2 bar), 30 kDa (2 bar) and 100 kDa (0.6 bar) filtrations are presented, because these three membranes can well represent low MWCO and high MWCO membranes according to the retention and recovery results (Section 3.2).

The red signals represent membrane surfaces and green signals represent QDs. For 1 kDa membranes, as it can be seen clearly from the cross-sectional views (*xz*, *yz*), QDs mainly accumulated on membrane surfaces, regardless of QDs sizes. Some regions of 1 kDa membranes were fully covered by QDs, but other regions were free of QDs or partially covered. This revealed that QDs distributed heterogeneously on 1 kDa membranes. Interestingly, from the top views (*xy*), it can be seen some blocks of green signals in 1 kDa membranes for relatively large QDs (CdTe-700). Apart from the possibility of membrane cracks or flaws, these blocks were supposed to be the large accumulation of QDs on membrane surfaces. But for other small QDs, more uniform deposits were found. This observation demonstrates that the structural morphologies of cake fouling layers between small and large QDs could be different, although all QDs were well retained by 1 kDa membranes.

For 30 and 100 kDa membranes, strong green signals inside membranes indicate that most QDs could penetrate high MWCO membranes, as seen from the cross-sectional views. These results are in good agreement with their corresponding retention and recovery results. Moreover, in some cases (e.g. CdTe-580 at 30 kDa–2 bar), it can be seen that green signals distributed uniformly inside membranes, possibly indicating a homogeneous distribution of QDs inside the membranes.

It should be noted that images presented in Fig. 5 correspond to a single membrane zone, and they provide qualitative information from one point of view, although these representative images were selected purposely. Therefore to gain more insights into QDs distributions in membranes, quantitative information from several membrane zones are needed, which will be discussed in the next section.

3.5. Distribution of QDs in different depths of membranes

3.5.1. Calculation methods: 'mean intensity' versus 'point intensity'

To calculate the distribution of QDs along membrane depths, two methods were used, both of which were based on fluorescence intensity values. Here, one example from 1 kDa filtration of CdTe-530 at 2 bar is shown in Fig. 6.

For 'mean intensity' method, the mean intensity values corresponding to membranes and QDs respectively in an area of 1.10×1.10 mm^2 (for each *xy* image) were given by CLSM software (Leica LAS AF). Then, the curves corresponding to mean intensity in *z*-series of images can be obtained (Fig. 6b). In the curve of membrane, the position on *z*-axis that gave the maximum intensity **(Imax)** value was assumed as the membrane surface ($z=0$ μm); the Imax-QDs value was supposed to represent the position where most QDs accumulated. Then, the distance from Imax-QDs to Imax-membrane surfaces can be calculated, to localize the maximum signals from QDs in depths of membrane. In Fig. 6b, it can be seen that CdTe-530 were mainly retained outside the 1 kDa membrane.

Alternatively, 'point intensity' method was used by choosing specific regions through Image J software (with protocols described in Section 2.5). In this way, oversaturated areas (gray value was over 255, the real intensity values cannot be obtained)

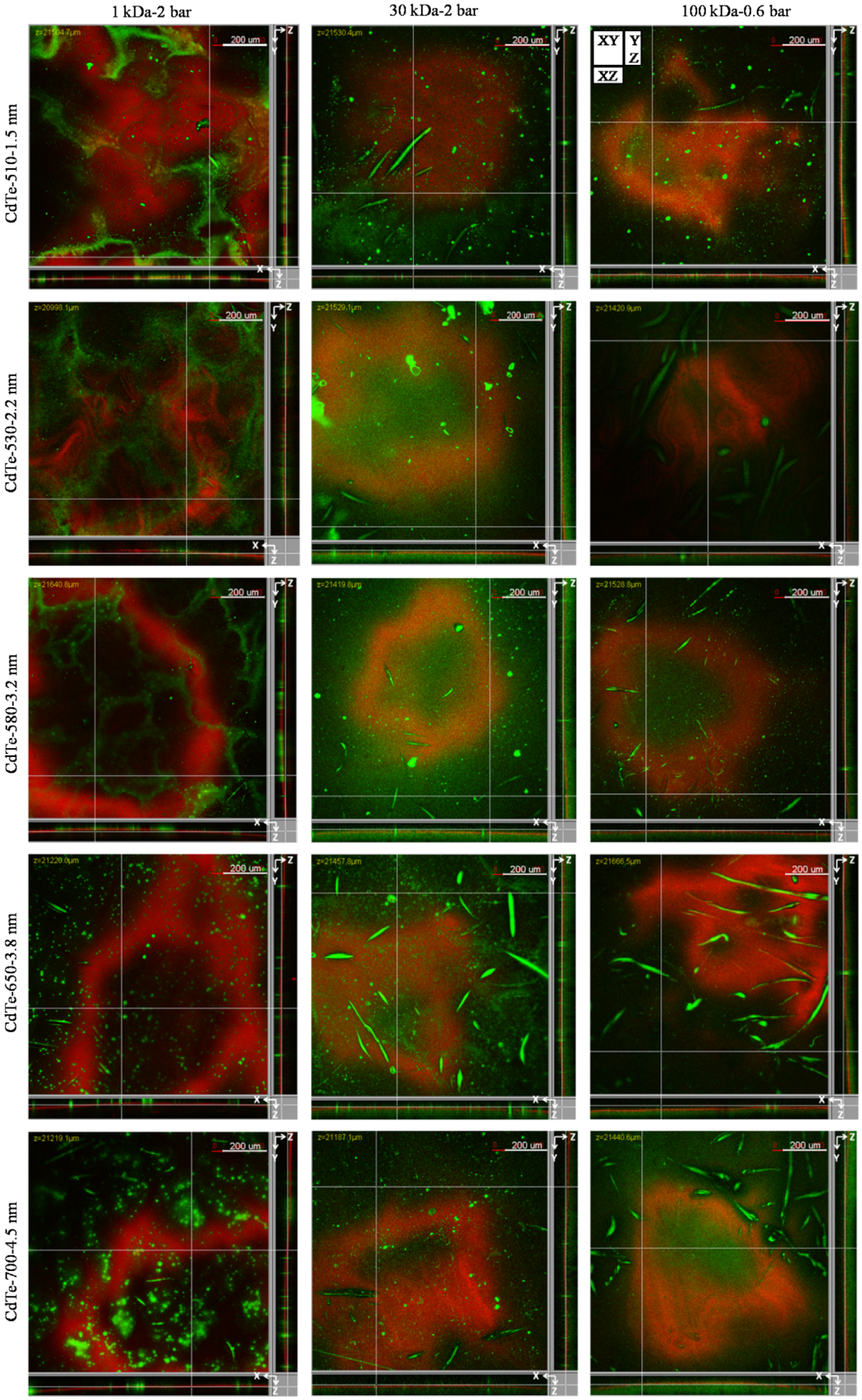

Fig. 5. Orthogonal view (*xy*, *xz*, *yz*) of reconstructed CLSM images obtained after filtrations of five QDs under different conditions (1 kDa at 2 bar, 30 kDa at 2 bar, and 100 kDa at 0.6 bar). Red indicates membranes and green indicates QDs. Scale bar = 200 μm. (For interpretation of the references to color in this figure legend, the reader is refered to the web version of this article.)

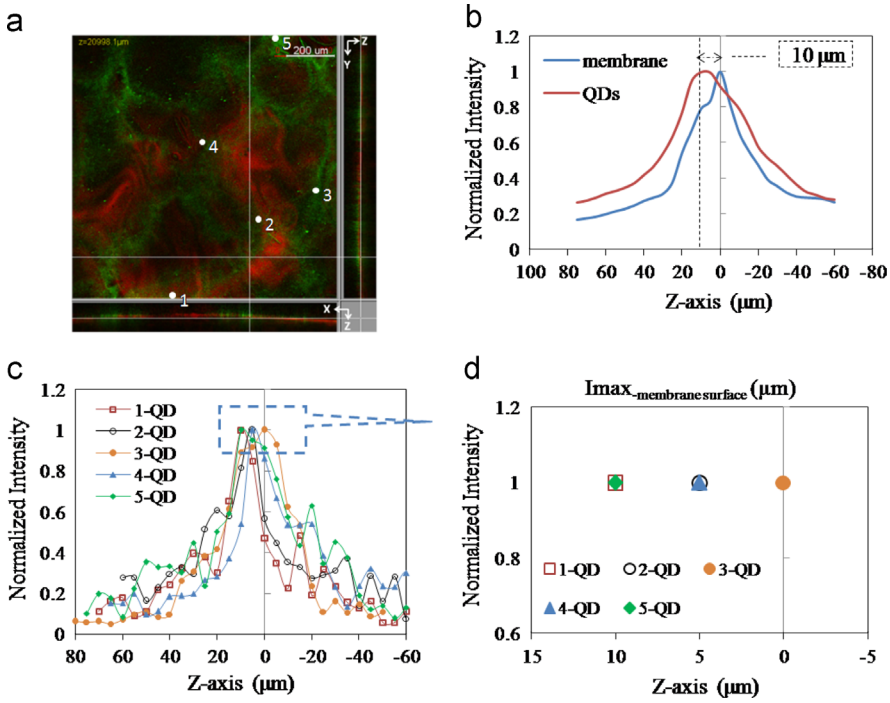

Fig. 6. Comparison of two calculation methods after 1 kDa filtration of CdTe-530 at 2 bar: (a) orthogonal view of 3D reconstructed CLSM images (b) mean intensity (c) point intensity (d) distances from maximum intensity (Imax) values of QDs to membrane surfaces. Negative *z*-axis values indicate the positions inside membranes.

can be avoided. Specifically, five points were randomly selected from cross-sectional images, given that QDs distributed heterogeneously in membranes. Because membranes were rarely found to be flat, the position of the membrane surface in each point needs to be calculated respectively. Then the curves corresponding to QDs intensity values along *z*-axis could be confirmed. As depicted in Fig. 6c, five curves corresponding to QDs presented the same tendency. But there exists some difference in distances from Imax-QDs to Imax-membrane surfaces.

To have a clear view, the positions of Imax-QDs were further enlarged (Fig. 6d), which showed that Imax-QDs occurred outside membranes ranging from 0 to 10 μm. The results obtained by 'point intensity' method are in good agreement with those obtained from 'mean intensity' method, even if there are fluctuations in QDs distribution profiles (Fig. 6c). This could be related to weak signals of QDs in specific chosen points.

3.5.2. *Distribution of QDs obtained from 'mean intensity'*

With the 'mean intensity' methodology, QDs distributions in membrane depths were determined. At the end of each filtration run, 4–6 different zones of fouled membrane were scanned by CLSM to give a comprehensive view of fouling pattern. The average values of normalized mean intensities corresponding to QDs from 4 to 6 zones are calculated as shown in Figs. 7–9. As mentioned previously, axial (*z*-axis) resolution of CLSM was about 7–8 μm. The interval of ±5 μm from $z=0$ μm is still considered as the position of the membrane surface during discussion of the following data.

3.5.2.1. 1, 5, 10 and 30 kDa membranes at TMP=2 bar. First, mean intensity curves of 1, 5, 10 and 30 kDa membranes are given for each type of QDs under TMP of 2 bar (Fig. 7).

For CdTe-510 (Fig. 7a), three curves representing 1, 5 and 10 kDa membranes were very similar, and their Imax-QDs (maximum intensity values) always occurred at the position of membrane surfaces ($z=0$ μm). The curve representing 30 kDa membrane shifted to the negative *z*-axis direction, which can be clearly differentiated from other three low MWCO membranes. This result is in good agreement with those obtained about retention (Fig. 4a) for which a significant decrease in retention is observed for 30 kDa membrane compared with 1, 5 and 10 kDa membranes. After $z=-5$ μm, CdTe-510 intensities in low MWCO membranes decreased more rapidly than in 30 kDa membranes, as penetration depth increased. The profile of CdTe-530 (Fig. 7b) was generally similar to CdTe-510. Only Imax-QDs positions in 30 kDa membranes were different between these two QDs. Specifically, for CdTe-530, Imax-QDs occurred inside 30 kDa membranes ($z=-15$ μm); while for CdTe-510, the presence of Imax-QDs was still in the field of the membrane surface ($z=-5$ μm).

For other three types of QDs at 2 bar (Fig. 7c–e), their Imax-QDs in low MWCO membranes mainly appeared around membrane surfaces (*z* from −5 to 5 μm); only for CdTe-650 (Fig. 7d), a thicker cake fouling layer was observed in 1 kDa filtration (Imax-QDs at $z=15$ μm), which could be dependent on the zones scanned (usually 4–6 different zones scanned in this study). In the case of 30 kDa membranes for these three types of QDs, their Imax-QDs positions were almost the same, which were next to the membrane surface ($z=-5$ μm). Additionally, for CdTe-580 and CdTe-700 (Fig. 7c and e), their 30 kDa curves can be clearly differentiated from other three low MWCO membranes, but not for CdTe-650 whose 30 kDa curve coincided with 5 kDa curve.

3.5.2.2. 10 and 30 kDa membranes at TMP=2 and 0.6 bar. For 10 kDa membranes, the mean intensity curves under two TMP are compared for each QDs (Fig. 8a–e). For most QDs, their 10 kDa intensity curves under two TMP were almost the same, and their positions of Imax-QDs were similar ranging from 0 to 5 μm. Only for CdTe-530 (Fig. 8b), the curve at high TMP (2 bar) shifted to the negative *z*-axis compared to low TMP (0.6 bar). This result might indicate a tendency that more CdTe-530 entered into 10 kDa membranes under high TMP than low TMP. Although it cannot be concluded that there was a significant difference between two Imax-QDs positions ($z=0$ μm at 2 bar and $z=5$ μm at 0.6 bar), due to the axial (*z*-axis) resolution of CLSM. For CdTe-580 (Fig. 8c), the

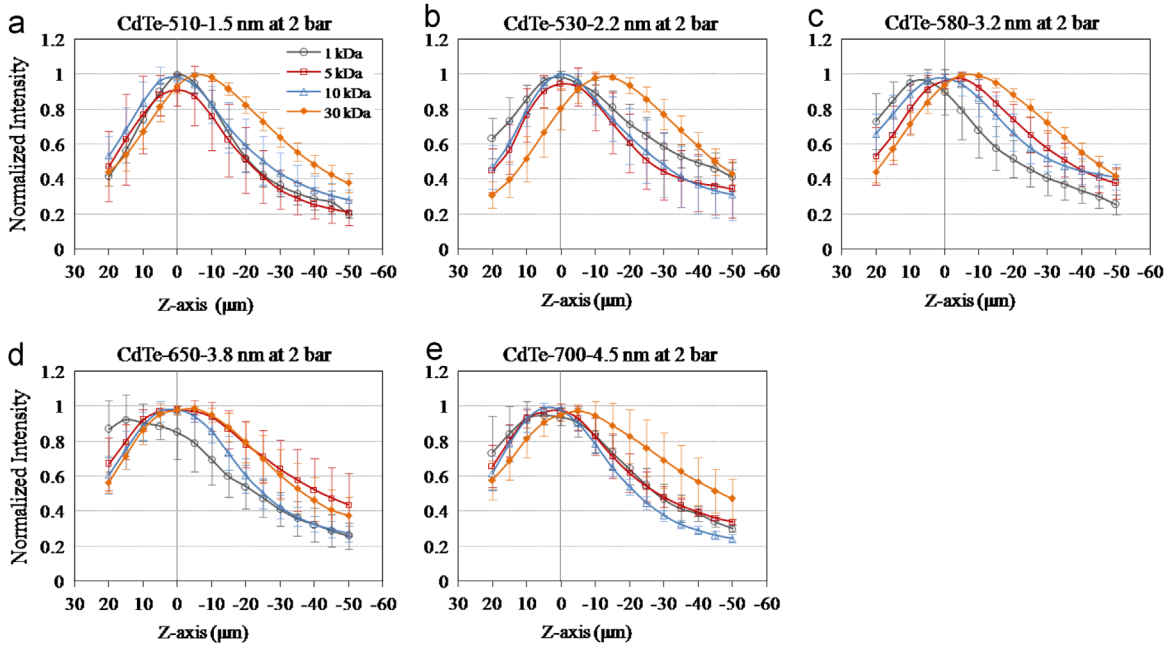

Fig. 7. Distribution of QDs in different depths of membranes obtained from mean intensity values (TMP=2 bar). Negative *z*-axis values indicate the positions inside membranes. Error bars refer to the standard deviations on the average of values from 4 to 6 different zones.

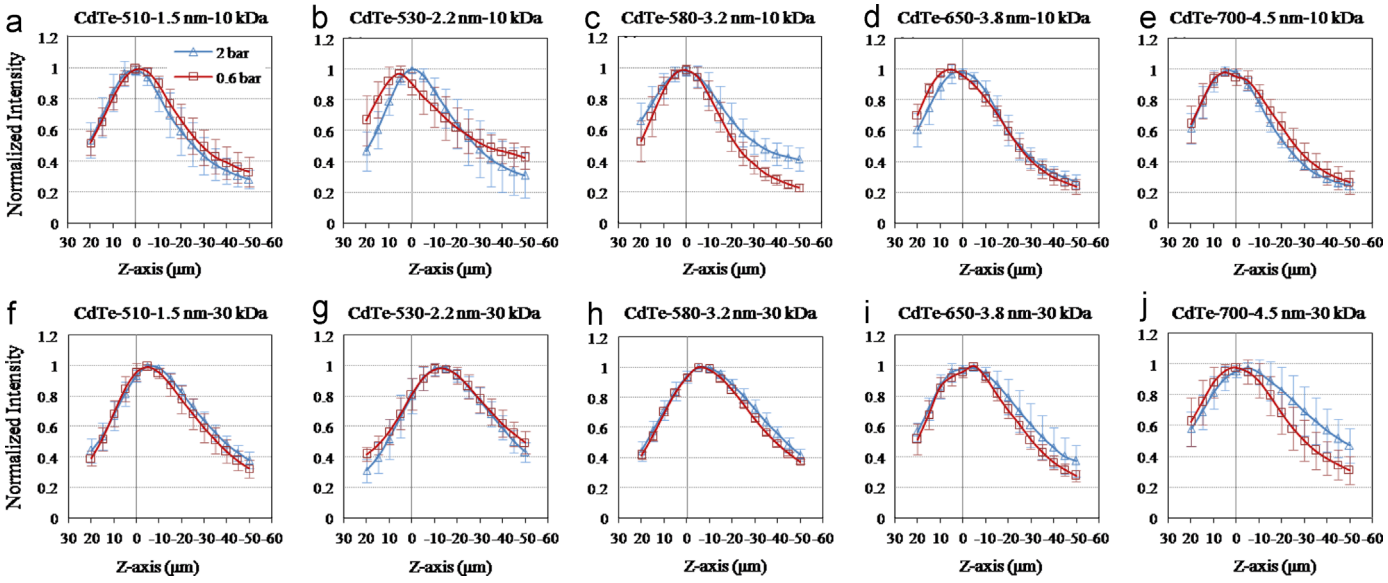

Fig. 8. Distribution of QDs in different depths of 10 and 30 kDa membranes obtained from mean intensity values (TMP=0.6 and 2 bar). Negative *z*-axis values indicate the positions inside membranes. Error bars refer to the standard deviations on the average of values from 4 to 6 different zones.

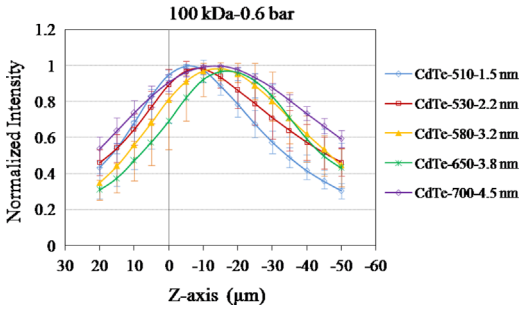

Fig. 9. Distribution of QDs in different depths of 100 kDa membranes obtained from mean intensity values (TMP=0.6 bar). Negative *z*-axis values indicate the positions inside membranes. Error bars refer to the standard deviations on the average of values from 4 to 6 different zones.

Imax-QDs positions of two curves were the same, but the curve of 0.6 bar was narrower than 2 bar. This result revealed that the distribution of CdTe-580 across 10 kDa membrane tended to be more concentrated under low TMP. However, this phenomenon was not observed for 10 kDa curves of other QDs.

Overall, the mean intensity curves of 10 kDa membranes were rarely influenced by TMP, and Imax-QDs often appeared at membrane surfaces. This tendency also agrees with the analysis of point intensity values in Section 3.5.3.

For 30 kDa membranes, the mean intensity curves under two different TMP are also compared for each QDs (Fig. 8f–j). Generally, the 30 kDa intensity curves under two TMP were very similar, indicating that the distribution of QDs in 30 kDa membranes was hardly influenced by TMP. This observation was in accordance with the results from 10 kDa membranes (Fig. 8a–e). For CdTe-650 and

CdTe-700 (Fig. 8i and j), their 30 kDa curves exhibited a more rapid decline inside membranes than those of smaller QDs. For example, normalized intensity of CdTe-530-0.6 bar (Fig. 8g) decreased to 0.5 until $z=-50$ μm, but the intensity of CdTe-700-0.6 bar (Fig. 8j) already decreased to 0.5 when $z=-30$ μm. This result demonstrated that the distribution of large QDs inside 30 kDa membranes was more concentrated than smaller QDs.

For most QDs, Imax-QDs occurred around 30 kDa membrane surfaces (usually $z=-5$ μm). Only for CdTe-530 (Fig. 8g), their positions of Imax-QDs were much lower at $z=-15$ μm, regardless of TMP.

3.5.2.3. 100 kDa membranes at TMP=0.6 bar. Finally, 100 kDa curves at TMP of 0.6 bar for all QDs are presented in Fig. 9. Imax-QDs in 100 kDa membranes normally occurred at deeper positions ($z=-10$ to -15 μm) away from membrane surfaces, compared with 10 and 30 kDa membranes. These results are in good agreement with those obtained about retention (Fig. 4b), where retention efficiencies in 100 kDa membrane were much lower than those exhibited by 10 and 30 kDa membranes. Imax-QDs was found at $z=-5$ μm only for CdTe-510. This indicates that CdTe-510 mainly deposited around 100 kDa membrane surfaces, which could be attributed to the adsorption of QDs to membranes or some internal fouling (e.g. standard blocking). Meanwhile, it should be taken into account that mean intensity method only provided an average value for each zone. During point intensity analysis, a wide distribution from -20 to 0 μm of Imax-QDs was found for CdTe-510 in 100 kDa membrane (Section 3.5.3.3).

Generally speaking, intensity curves representing high MWCO membranes shifted to negative z-axis, compared to low MWCO membranes. These results revealed that QDs usually penetrate inside membranes to deeper positions with increasing membrane MWCO. Additionally, no significant influence of TMP was observed on QDs distributions in 10 and 30 kDa membranes according to mean intensity curves. These results are in agreement with those obtained about retention and recovery for 10 kDa membranes (Fig. 4).

3.5.3. Distribution of QDs obtained from 'point intensity'

As discussed previously, to obtain comprehensive information about QDs distribution in membranes, the values Imax-QDs positions were calculated using 'point intensity' method. In Figs. 10–12, the box charts summarized the variation of Imax-QDs positions. For each filtration process, the values were obtained from 4 to 6 zones and three different points for each zone (12–18 values for each box). Through these box plots, data distributions for Imax-QDs positions can be compared between different groups.

3.5.3.1. 1, 5, 10 and 30 kDa membranes at TMP=2 bar. For CdTe-510 at 2 bar (Fig. 10a), Imax-QDs positions in low MWCO membranes were generally the same which appeared around membrane surfaces or on the top of membranes up to 10 μm. These results are in good agreement with those obtained from 'mean intensity' method. Imax-QDs positions in 30 kDa membranes were generally deeper (mean values about -10 μm) than those in low membranes, but showed a wider distribution from -25 to 5 μm. This means that fouling positions of CdTe-510 in 30 kDa membranes were variable, dependent on membrane regions. For other four types of QDs at 2 bar (Fig. 10b–e), they presented similar tendencies like CdTe-510, whose Imax-QDs positions in 30 kDa membranes (from -25 to 5 μm) were usually lower than in low MWCO membranes (from -10 to 20 μm).

3.5.3.2. 10 and 30 kDa membranes at TMP=2 and 0.6 bar. In terms of 10 kDa membranes, the impact of TMP (0.6 bar and 2 bar) on Imax-QDs positions are compared (Fig. 11a–e). For CdTe-580 and CdTe-700 (Fig. 11c and e), data distributions obtained under two TMP were almost the same, indicating that there was no impact of TMP on their Imax-QDs positions. For other QDs, the difference in Imax-QDs distributions was not significant between two TMP (within ± 5 μm). Overall, Imax-QDs occurred mainly around 10 kDa membrane surfaces or on top of membranes (z from -5 to 10 μm), but low values of -10 μm were also observed occasionally which could be related to the points selected. In most cases, Imax-QDs positions in 10 kDa membranes were hardly influenced by TMP, which agreed with results from mean intensity methods.

For 30 kDa membranes (Fig. 11f–j), the Imax-QDs distributions were normally comparable between two TMP for these QDs. The results indicated that TMP had limited impact on Imax-QDs

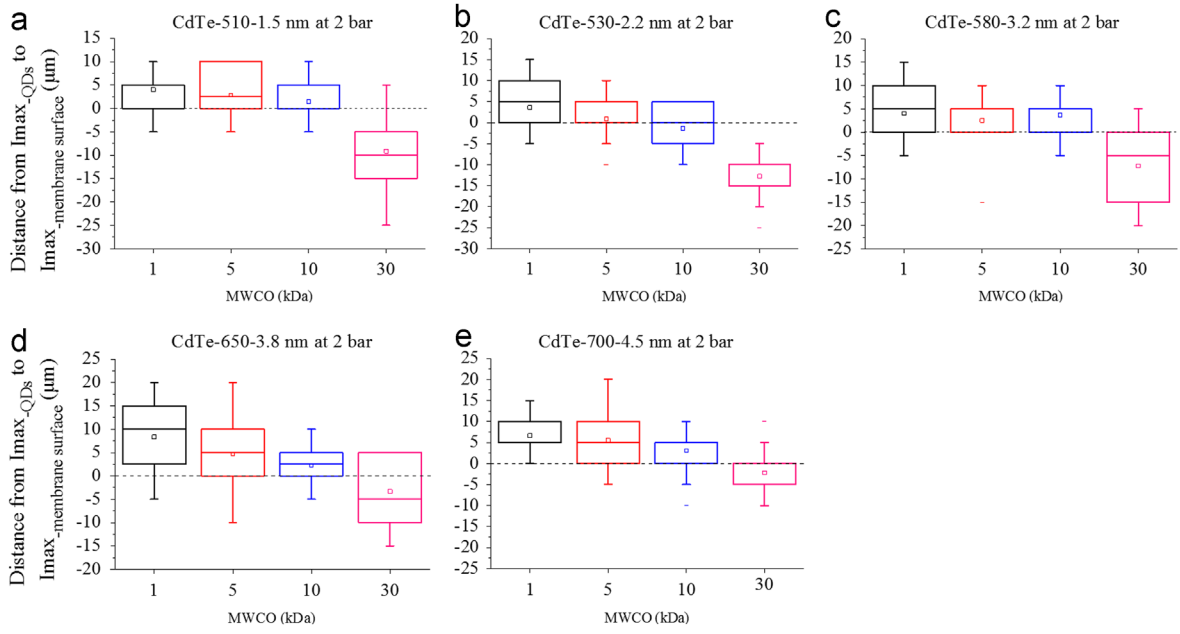

Fig. 10. Distances from maximum intensity (Imax) values of QDs to membrane surfaces obtained under TMP of 2 bar (12–18 values for each box). The top and bottom of each box represent 75th and 25th percentiles, respectively; the top and bottom of each whisker represent 95th and 5th percentiles, respectively; line across inside each box represents median value; the small square represents the mean value.

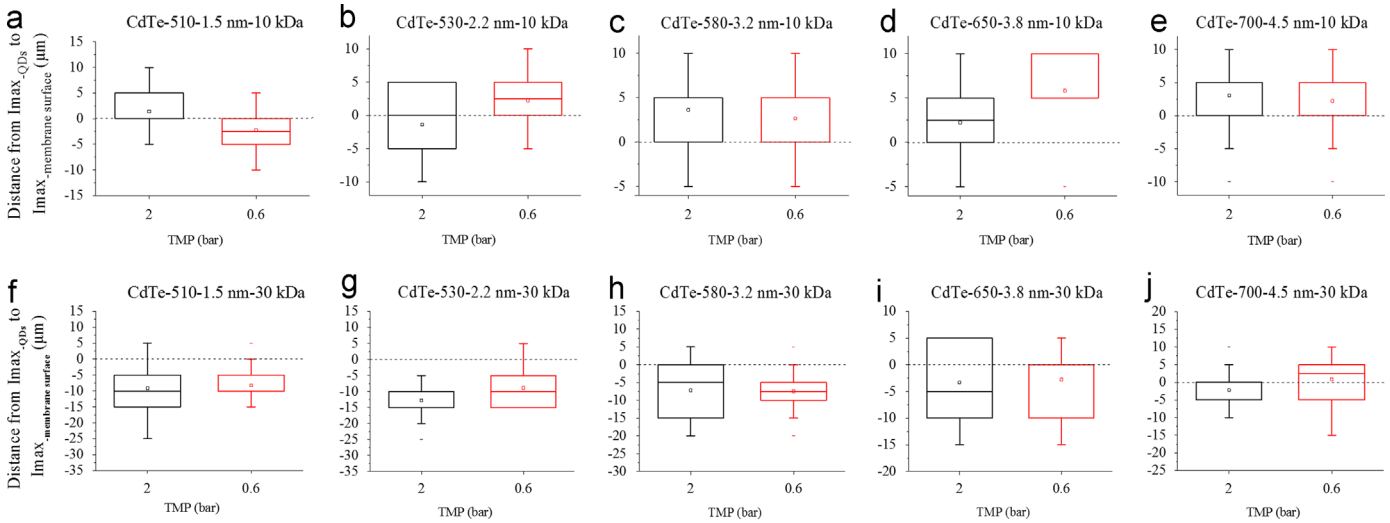

Fig. 11. Distances from maximum intensity (Imax) values of QDs to 10 and 30 kDa membrane surfaces obtained under two TMP (12–18 values for each box). The top and bottom of each box represent 75th and 25th percentiles, respectively; the top and bottom of each whisker represent 95th and 5th percentiles, respectively; line across inside each box represents median value; the small square represents the mean value.

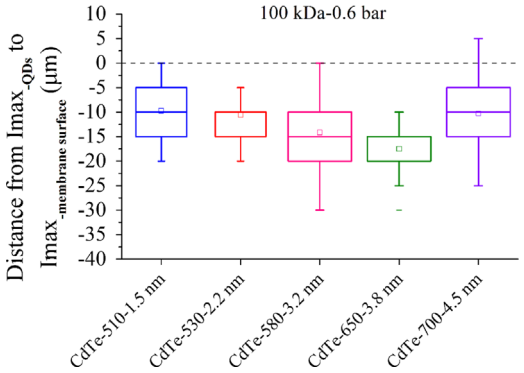

Fig. 12. Distances from maximum intensity (Imax) values of QDs to 100 kDa membrane surfaces obtained under TMP of 0.6 bar (12–18 values for each box). The top and bottom of each box represent 75th and 25th percentiles, respectively; the top and bottom of each whisker represent 95th and 5th percentiles, respectively; line across inside each box represents median value; the small square represents the mean value.

positions in 30 kDa membranes, corresponding to their 'mean intensity' results. Imax-QDs were generally found inside 30 kDa membranes or around membrane surfaces, ranging from −25 to 5 μm. But up to 10 μm of position was also observed for CdTe-700 (Fig. 11j).

3.5.3.3. 100 kDa membranes at TMP=0.6 bar. In 100 kDa membranes, the positions of Imax-QDs were generally found inside membranes or around membrane surfaces, ranging from −30 to 5 μm (Fig. 12). Only considering the mean values (small square in the box), Imax-QDs positions presented a gradual decrease with increasing QDs sizes, from −10 μm (CdTe-510 and CdTe-530) to about −18 μm (CdTe-650). But for CdTe-700 with the largest sizes, its mean value of Imax-QDs position was about -10 μm like CdTe-510 and CdTe-530. For smaller particles, CdTe-510 and CdTe-530, their relatively shallower Imax-QDs positions might be attributed to adsorption to membrane pores. For larger particles, CdTe-700, the shallower Imax-QDs positions could be attributed to large particle sizes.

Totally, results from 'point intensity' method were in well accordance with those obtained from 'mean intensity' method, and 'point intensity' method provided a wider range of values than 'mean intensity' method. Additionally, when combined with retention results, it can be found that for low MWCO membranes, Imax-QDs distributed mainly around surfaces or on top of membranes, accompanied with near 100% retention. As membrane MWCO increased (30 and 100 kDa), more QDs could pass through membranes accompanied with decreasing retention efficiencies, and the occurrence of Imax-QDs was usually in deeper positions of membranes at the same time.

For all membranes, QDs presented in the permeate sides of membranes and/or into membrane skins, but the presence of QDs in the support layers cannot be detected in this study. This observation is in agreement with fouling analysis which demonstrated the occurrence of both internal and external fouling.

4. Conclusions

As a conclusion, in this study, the filtrations of five types of CdTe QDs with different sizes (from 1 to 5 nm) were performed by using five MWCO membranes (from 1 to 100 kDa) under two different TMP (0.6 bar and 2 bar). For each filtration run, several aspects were evaluated including retention and recovery efficiencies, filtration data and CLSM analysis. The results obtained from different aspects were in good agreement with each other. On this basis, the impact of membrane MWCO and TMP on separation of QDs was evaluated.

The new methodology developed in this study (QDs preparation, filtration processes, CLSM and image analysis) was successfully applied to get qualitative and quantitative information about membrane fouling by nanoparticles. The methods ('mean intensity' and 'point intensity') developed to localize QDs along membrane depths are rapid and user-friendly. The spatial distributions of QDs in membranes (e.g. the positions of Imax-QDs) were also in well accordance with corresponding retention/recovery results and fouling analysis. Although the acquisition of very precise information about QDs distribution is hindered by low resolution and limited penetration depth, the results obtained provide very useful information on QDs distribution in membranes and improve the understanding about how ENMs are retained by membranes. However, it should be pointed out that this part focuses on the synthetic nanoparticles (negative QDs) in simple matrix (ultrapure water). Results obtained under simplified conditions are valuable for understanding the membrane fouling caused by ENMs, but are not applicable to most natural waters due to their complex matrix.

So experiments with solutions containing mineral salts, organic matter, suspended matter and/or mixture of QDs are in progress and will be presented in a forthcoming paper.

All studies were performed with rigid, spherical QDs. It would be relevant to comment about the potential impact of nanoparticles with a 'softer', deformable structure (that may occur in various environmental conditions), in particular because they may form cake layers with a completely different (compressible) behavior when filtered by membranes. In addition, the experiments were only tested under constant TMP. In the case of filtrations under controlled permeate flux, the results and conclusions might be different, such as membrane fouling patterns. Further studies need to be conducted to determine the impact of controlled parameters.

Acknowledgments

The authors would like to thank the Labex MEC for financial support. Thanks to Y.P. Liu, P.L. Artufel and H. Li for their help during experiments.

References

[1] R. Kaegi, A. Ulrich, B. Sinnet, R. Vonbank, A. Wichser, S. Zuleeg, H. Simmler, S. Brunner, H. Vonmont, M. Burkhardt, M. Boller, Synthetic TiO_2 nanoparticle emission from exterior facades into the aquatic environment, Environ. Pollut. 156 (2008) 233–239.
[2] N. Wu, Y. Wyart, Y. Liu, J. Rose, P. Moulin, An overview of solid/liquid separation methods and size fractionation techniques for engineered nanomaterials in aquatic environment, Environ. Technol. Rev. 2 (1) (2013) 55–70.
[3] D.A. Ladner, M. Steele, A. Weir, K. Hristovski, P. Westerhoff, Functionalized nanoparticle interactions with polymeric membranes, J. Hazard. Mater. 211–212 (2012) 288–295.
[4] F. Springer, S. Laborie, C. Guigui, Removal of SiO_2 nanoparticles from industry wastewaters and subsurface waters by ultrafiltration: investigation of process efficiency, deposit properties and fouling mechanism, Sep. Purif. Technol. 108 (2013) 6–14.
[5] C. Henry, J.A. Brant, Mechanistic analysis of microfiltration membrane fouling by buckminsterfullerene (C_{60}) nanoparticles, J. Membr. Sci. 415–416 (2012) 546–557.
[6] J. Lohwacharin, S. Takizawa, Effects of nanoparticles on the ultrafiltration of surface water, J. Membr. Sci. 326 (2009) 354–362.
[7] S.F. Wuister, I. Swart, F. van Driel, S.G. Hickey, C. de Mello Donegá, Highly luminescent water-soluble CdTe quantum dots, Nano Letters 3 (2003) 503–507.
[8] H. Montón, C. Nogués, E. Rossinyol, O. Castell, M. Roldán, QDs versus Alexa: reality of promising tools for immunocytochemistry, J. Nanobiotechnol. 7 (2009) 1–10.
[9] J.B. Morrow, C. Arango, R.D. Holbrook, Association of quantum dot nanoparticles with *Pseudomonas aeruginosa* biofilm, J. Environ. Qual. 39 (2010) 1934–1941.
[10] M. Ferrando, A. Rožek, M. Zator, F. López, C. Güell, An approach to membrane fouling characterization by confocal scanning laser microscopy, J. Membr. Sci. 250 (2005) 283–293.
[11] M. Zator, M. Ferrando, F. López, C. Güell, Membrane fouling characterization by confocal microscopy during filtration of BSA/dextran mixtures, J. Membr. Sci. 301 (2007) 57–66.
[12] M. Peter-Varbanets, F. Hammes, M. Vital, W. Pronk, Stabilization of flux during dead-end ultra-low pressure ultrafiltration, Water Res. 44 (2010) 3607–3616.
[13] Y. Hao, C. Liang, A. Moriya, H. Matsuyama, T. Maruyama, Visualization of protein fouling inside a hollow fiber ultrafiltration membrane by fluorescent microscopy, Ind. Eng. Chem. Res. 51 (2012) 14850–14858.
[14] C. Sun, L. Fiksdal, A. Hanssen-Bauer, M.B. Rye, T. Leiknes, Characterization of membrane biofouling at different operating conditions (flux) in drinking water treatment using confocal laser scanning microscopy (CLSM) and image analysis, J. Membr. Sci. 382 (2011) 194–201.
[15] A. Bjørkøy, L. Fiksdal, Characterization of biofouling on hollow fiber membranes using confocal laser scanning microcscopy and image analysis, Desalination 245 (2009) 474–484.
[16] B.-K. Hwang, W.-N. Lee, P.-K. Park, C.-H. Lee, I.-S. Chang, Effect of membrane fouling reducer on cake structure and membrane permeability in membrane bioreactor, J. Membr. Sci. 288 (2007) 149–156.
[17] P.A. Neale, Influence of solute–solute interactions on membrane filtration, (Ph.D. dissertation), University of Edinburgh, 2009.
[18] A.I. Schäfer, Natural organics removal using membranes (Ph.D. dissertation), University of New South Wales, 1999.
[19] E. Abbe, On the estimation of aperture in the microscope, J. R. Microsc. Soc. 1 (1881) 388–423.
[20] I.R. Quevedo, N. Tufenkji, Mobility of functionalized quantum dots and a model polystyrene nanoparticle in saturated quartz sand and loamy sand, Environ. Sci. Technol. 46 (2012) 4449–4457.
[21] I.R. Quevedo, N. Tufenkji, Influence of solution chemistry on the deposition and detachment kinetics of a CdTe quantum dot examined using a quartz crystal microbalance, Environ. Sci. Technol. 43 (2009) 3176–3182.
[22] J. Hermia, Constant pressure blocking filtration laws—application to power-law non-Newtonian fluids, Trans. Inst. Chem. Eng. 60 (1982) 183–187.
[23] Y. El Rayess, C. Albasi, P. Bacchin, P. Taillandier, M. Mietton-Peuchot, A. Devatine, Analysis of membrane fouling during cross-flow microfiltration of wine, Innov. Food Sci. Emerg. 16 (2012) 398–408.
[24] S. Giglia, G. Straeffer, Combined mechanism fouling model and method for optimization of series microfiltration performance, J. Membr. Sci. 417–418 (2012) 144–153.